DRAC

Durcan, Julie A.; King, Georgina Elizabeth; Duller, Geoffrey A T

Published in:
Quaternary Geochronology

DOI:
10.1016/j.quageo.2015.03.012

Publication date:
2015

Citation for published version (APA):
Durcan, J. A., King, G. E., & Duller, G. A. T. (2015). DRAC: Dose Rate and Age Calculator for trapped charge dating. *Quaternary Geochronology*, *28*, 54-61. https://doi.org/10.1016/j.quageo.2015.03.012

DRAC: Dose Rate and Age Calculator for trapped charge dating

Julie A. Durcan [a*], Georgina E. King [b,c*], Geoffrey A.T. Duller [c]

[a] School of Geography and the Environment, University of Oxford, Oxford, OX1 3QY, UK.
[b] Institute of Earth Surface Dynamics, University of Lausanne, Lausanne, Switzerland.
[c] Department of Geography and Earth Sciences, Aberystwyth University, Aberystwyth, SY23 3DB, UK.
[*] corresponding authors. Email julie.durcan@ouce.ox.ac.uk and georgina.king@unil.ch

Full reference: Durcan, J.A., King, G.E., Duller, G.A,T., 2015. DRAC: Dose rate and age calculator for trapped charge dating. Quaternary Geochronology, 28, 54-61. doi:10.1016/j.quageo.2015.03.012.

Highlights

- DRAC is a Dose Rate and Age Calculator for trapped charge dating.
- DRAC is available online at www.aber.ac.uk/alrl/drac.
- DRAC enables easy and transparent dose rate calculation.
- Users input sample details and select appropriate factors to calculate dose rates.
- Users download an output table detailing inputs and all calculated values.

Abstract

Accurate calculation of the environmental radiation dose rate (Ḋ) is an essential part of trapped charge dating methods, such as luminescence and electron spin resonance dating. Although the calculation of Ḋ is not mathematically complex, the incorporation of multiple variables and the propagation of uncertainties can be challenging. The Dose Rate and Age Calculator (DRAC) is an open access, web-based program which enables rapid Ḋ calculation for trapped charge dating applications. Users can select from recently published attenuation and conversion factors to make mathematically robust, reproducible Ḋ calculations. Comparison of DRAC calculated Ḋ values against the published Ḋ determinations of 422 samples from 32 studies results in a reproducibility ratio of 1.01 ± 0.05. It is anticipated that DRAC will facilitate easier inter-laboratory comparisons and will provide greater transparency for Ḋ calculations. DRAC will be updated to reflect the latest advances in Ḋ calculation and is freely accessible at www.aber.ac.uk/alrl/drac. The code for DRAC is available from GitHub at https://github.com/DRAC-calculator/DRAC-calculator.

Keywords: DRAC; Dose rate; Age; Calculator; Luminescence dating; Electron spin resonance dating; Software; Open access.

1. Introduction

Trapped charge dating techniques such as luminescence and electron spin resonance (ESR) dating are key Quaternary dating methods and in a period of 22 months from January 2013, over 500 papers have been published using these techniques. Within luminescence dating, calculation of the environmental dose rate (Ḋ) is equally important as calculation of the equivalent dose (D_e) in age determinations, yet many luminescence dating publications tend to be more focused upon the calculation of D_e values. The recent luminescence laboratory inter-comparison project (Buylaert et al., 2006 and Murray et al., 2015) initially reported at the UK Luminescence meeting held in Aberystwyth in September 2012, highlighted that whilst D_e values are measured reproducibly between different laboratories, greater variability is seen in Ḋ

determinations. This may be partly explained by the variety of measurement techniques used to infer Ḋ, i.e. some laboratories use techniques to determine radionuclide concentrations (e.g. inductively-coupled plasma mass spectrometry (ICP-MS)), whereas other laboratories use emission counting methods to directly measure radioactivity. However, De Corte et al. (2007) compared a wide range of different methods for dose rate determination and did not record major differences between techniques. An alternative explanation is variability in the parameters used in Ḋ determinations, such as different radionuclide conversion factors (e.g. Adamiec and Aitken, 1998 and Guerin et al., 2012) and dose rate attenuation factors (e.g. Brennan, 2003 and Mejdahl, 1979), which will result in minor variability in the calculated Ḋ. Furthermore, although the mathematics required in the dose rate calculation is not complex, the compilation of in excess of 10 variables (Fig. 1) provides many opportunities for miscalculation. To overcome the challenges of Ḋ calculation, desktop based programs have been previously published e.g. the AGE program (Grün, 2009). However as this program is written to be run in a DOS based language it requires additional DOS emulation software to run in versions of Windows more recent than XP and the radionuclide conversion factors it uses have now been superseded. Other programs have not been formally published (e.g. ADELE; Kulig, 2005) and are not widely available. We present here a web-based Dose Rate and Age Calculator (DRAC), which is freely available and can be more easily updated to reflect the most recent conversion and attenuation factor publications. By providing a standardised calculator with transparent calculations which utilises published input variables, DRAC provides an effective means of removing the potential for miscalculation and will facilitate improved assessment of dose rate and age calculations and more simple inter-laboratory Ḋ comparisons.

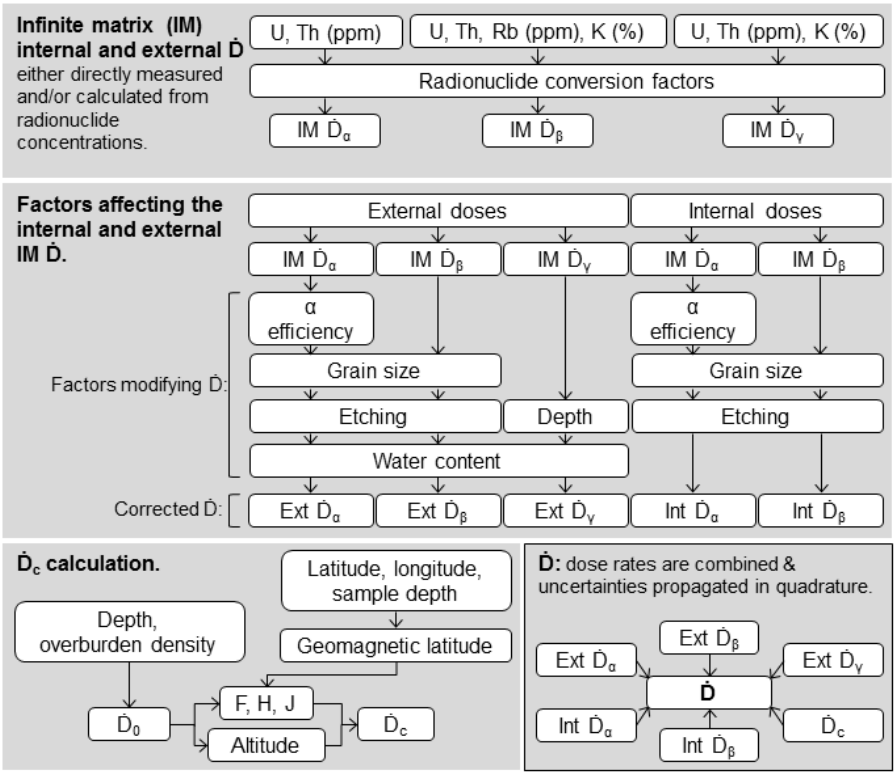

Figure 1: Overview of the Ḋ calculation for trapped charge dating applications. IM – infinite matrix, ext – external, int – internal.

2. DRAC website and data input

DRAC (v1.1) can be accessed at www.aber.ac.uk/alrl/drac and is hosted by the Aberystwyth Luminescence Research Laboratory, Aberystwyth University, UK. The publication of DRAC as a website ensures that users

will immediately benefit from software updates, and that revised inputs can be rapidly incorporated into the calculation code. A key objective of DRAC is calculation transparency, and it is intended that all users will be able to easily trace the methods used to calculate published dose rate values in a similar manner to the cosmogenic nuclide dating community, who have recently benefitted from the development of CRONUS (Balco et al., 2008). Therefore, the DRAC calculation code is listed on GitHub which is an open access code repository, and can be accessed using a link from the DRAC website.

The DRAC website is comprised of three key parts: a user guide, the calculator input page, and the data tables summary. The user guide page provides a short introduction to the calculation process used by DRAC and provides a summary of the inputs required and outputs generated by DRAC. On the calculator input page, users can download a .csv template of the inputs required for the dose rate calculation, and once this has been populated, can copy and paste their data into the calculation box. Note that because this comprises a text input, it is important to ensure that values are input with the correct number of significant figures. DRAC users can input data for multiple samples by populating multiple rows of data, facilitating the rapid analysis of a number of samples simultaneously. Once users click "calculate", DRAC produces an output file in .csv format which provides a summary table, as well as listing all of the inputs used, the variables that have been selected (e.g. a-value, grain size etc.) and calculated values (e.g. the different attenuation factors). Input and output tables populated with example data are provided in the Supplementary Information for reference, although users should always refer to the DRAC website to ensure they are using the most up to date versions of the input and output tables. The data tables page provides the datasets (e.g. conversion factors, attenuation factors) that can be selected and used in the $\dot{D}$ calculation. These datasets are also detailed in the Supplementary Information.

3. Determination of the environmental dose rate ($\dot{D}$)

Four types of radiation contribute to the $\dot{D}$ received by a sample: alpha particles (α), beta particles (β), gamma rays (γ) and cosmic rays. The dose rate from each of these sources is combined to calculate the total $\dot{D}$, which is used in trapped charge dating calculations. The alpha ($\dot{D}_\alpha$), beta ($\dot{D}_\beta$) and gamma ($\dot{D}_\gamma$) dose rates originate from naturally occurring radionuclides, including Uranium (U), Thorium (Th) and Potassium (K), which are present in the surrounding sediment matrix and make up a proportion of the crystalline structure of some minerals. The radiation emitted can be attenuated due to a variety of factors including grain size and sediment-matrix water content, requiring that dose rates are adjusted. The cosmic dose rate ($\dot{D}_c$) received by a sample is a function of the geographic location, burial depth and altitude from which the sample was taken. In DRAC, the internal and external dose rates are calculated and attenuated as appropriate, and along with the $\dot{D}_c$, these are combined to calculate the total $\dot{D}$. The calculation stages are discussed below.

3.1. External alpha, beta and gamma dose rates

Aitken (1985a) comments that for the majority of samples, U, Th and K comprise almost all of the total $\dot{D}$ in approximately equal parts, with a small contribution from Rubidium (Rb) and the $\dot{D}_c$. Dose rates resulting from the decay of these elements can be calculated either by determining the radionuclide concentrations present in the sediment matrix or by directly measuring the emission of radiation from the sediment (cf. De Corte et al., 2007). Many measurement techniques are available for dose rate determination, including ICP-MS, neutron activation analysis, gamma spectrometry, thick source alpha and beta counting, and alpha spectroscopy.

DRAC offers the flexibility of inputting either radionuclide concentrations and/or directly measured dose rates. Alternatively, a combination of the two can be used, e.g. the $\dot{D}_\beta$ may be measured directly using beta counting, whilst the $\dot{D}_\alpha$ and $\dot{D}_\gamma$ are determined from radionuclide concentrations. Where the user inputs a combination of radionuclide concentrations and directly measured dose rates, DRAC will use the specified dose rate in calculations. These specified dose rates should be input in $Gy.ka^{-1}$, and will be attenuated by DRAC in subsequent calculation stages. Users will note from Table S1 that radionuclide concentrations of U, Th and Rb should be input in ppm and K in %. Details of how to convert from $Bq.kg^{-1}$ to ppm and K_2O% to K are detailed in the Supplementary Information (Table S3.1). Where the user opts to use radionuclide concentrations for dose rate calculations, they have the option of either inputting a Rb concentration or deriving Rb from the K concentration, where Rb (ppm) is equal to −9.17 + 38.13 K (%) after Mejdahl (1987).

3.1.1. Radionuclide conversion factors

A set of conversion factors are used to calculate the infinite-matrix alpha, beta and gamma dose rates derived from a radionuclide. Conversion factors for each radionuclide derived from nuclear data tables have been published by a number of authors (e.g. Adamiec and Aitken, 1998). Liritzis et al. (2013) have most recently updated the conversion factors from values previously published by Guerin et al. (2011) and Adamiec and Aitken (1998). In contrast to previous contributions, Liritzis et al. (2013) have also calculated uncertainties for their conversion factors and in the absence of calculated uncertainties in the studies of Guerin et al. (2011) and Adamiec and Aitken (1998), proportional uncertainties derived from Liritzis et al. (2013) are applied to all three datasets. The data tables used in DRAC can be viewed in the Supplementary Information accompanying this paper (Table S3.2) and on the DRAC website. Radionuclide concentrations are multiplied by the relevant conversion factor to determine the $\dot{D}_\alpha$, $\dot{D}_\beta$ and $\dot{D}_\gamma$ delivered by the decay of each element. The uncertainties are propagated in quadrature when calculating the dose rate from each of the radionuclides. Further details of the calculation process and worked examples are presented in the Supplementary Information (S3.9, S3.10, and S3.11).

3.2. Internal alpha and beta dose rates

The inclusion of U, Th and K within the mineral lattice of quartz and feldspar grains results in an internal $\dot{D}_\alpha$and $\dot{D}_\beta$ component, which is particularly significant for K-feldspars. For quartz, Aitken (1998) suggests that in most environments, the contribution of the internal alpha dose rate to the $\dot{D}$ is negligible, particularly given its low alpha efficiency (Rees-Jones and Tite, 1997). However, in some environments with low environmental dose rates, internal doses for quartz may account for a few percent of the total dose rate (e.g. Armitage and King, 2013, Jacobs et al., 2003 and Sutton and Zimmerman, 1978). Users of DRAC working in low dose environments can incorporate a user-defined and attenuated internal $\dot{D}$ within their dose rate calculation (e.g. Vandenberghe et al., 2008) if required. The inclusion of K within the structure of K-feldspars results in an internal $\dot{D}_\beta$ (e.g. Huntley and Baril, 1997) and the recent development of the post-IR IRSL protocol (Buylaert et al., 2009 and Thomsen et al., 2008) and technological advances that facilitate single-grain K-feldspar dating, have resulted in efforts to precisely measure individual-grain internal K contents (e.g. Smedley et al., 2012). In DRAC, users should input a K concentration value for their samples or may wish to use the K content values of 12.5 ± 0.5% of Huntley and Baril (1997) or the 10 ± 2% measured by Smedley et al. (2012).

In DRAC, users can input internal radionuclide concentrations of U, Th and K which will be multiplied by the selected conversion factors to calculate the internal $\dot{D}_\alpha$ and $\dot{D}_\beta$, and which will be adjusted for grain size. The internal $\dot{D}_\alpha$ will also be adjusted for alpha efficiency. Alternatively, users may input a specified internal

Ḋ (Gy.ka^{-1}) which should be the sum of both the internal $\dot{D}_{\alpha}$ and $\dot{D}_{\beta,}$ user defined internal dose rates, and must be provided in a grain-size attenuated form, because without specified radionuclide concentrations it is not possible for DRAC to calculate an appropriate attenuation factor.

3.3. Attenuation factors

In order to determine the Ḋ from the calculated internal and external $\dot{D}_{\alpha}$, $\dot{D}_{\beta}$ and $\dot{D}_{\gamma}$, it is necessary to adjust the doses for a range of factors, including alpha efficiency, grain size, removal of the grain surface by etching, and moisture content. DRAC users can select from a variety of published datasets for attenuation of dose rates, as detailed below.

3.3.1. Alpha efficiency (a-value)

In contrast to beta particles and gamma rays, alpha particles are highly ionising and cause the saturation of trapping defects within their alpha decay tracks (Aitken, 1985a). This is corrected for by using an alpha efficiency factor, or a-value (Aitken and Bowman, 1975), which can be considered as the ratio of luminescence per unit alpha track length to the luminescence per unit absorbed beta dose (Aitken, 1985b). A range of a-values have been published in the literature for different grain-sizes and mineral types, and within DRAC, users should input their selected a-value for any samples where an alpha contribution is to be calculated. The most commonly used published values include 0.15 ± 0.05 for coarse-grained K-feldspar (Balescu and Lamothe, 1994), 0.10 ± 0.02 for coarse-grained quartz (Olley et al., 1998), 0.038 ± 0.002 for fine-grained quartz (Rees-Jones, 1995) and 0.086 ± 0.004 for polymineral fine grains (Rees-Jones, 1995), but see also Lai et al., 2008, Lang, 1994 and Mauz et al., 2006 and Spooner et al. (1990) for other values. If an a-value is provided, the user defined external $\dot{D}_{\alpha}$, or the dose rate calculated from U and Th concentrations will be adjusted accordingly.

3.3.2. Grain size

The range of alpha and beta particles may be comparable with the diameter of the grains under investigation, therefore dose rates must be corrected for grain-size attenuation effects. Bell (1980) calculated attenuation factors for alpha dose rates from U and Th for quartz, and more recently Brennan et al. (1991) calculated alpha attenuation factors for spherical grains, accounting for alpha track length. The attenuation factors of Brennan et al. (1991) are greater than those of Bell (1980) (Fig. 2), however as the factors of Bell (1980) have remained in widespread use throughout OSL publications over the past ~30 years, users may select from either set of attenuation factors in DRAC. For $\dot{D}_{\beta}$ grain size attenuation, DRAC users can choose between four datasets: Mejdahl, 1979 and Brennan, 2003, and Guerin et al. (2012) who offer two sets of factors, one for quartz and one for feldspar (Fig. 3). If a Rb concentration has been provided or calculated, the dataset of Readhead, 2002a and Readhead, 2002b will be used to attenuate the $\dot{D}_{\beta}$ from Rb. The different sets of attenuation factors assume grain sphericity, infinite matrix homogeneity and radionuclide equilibrium.

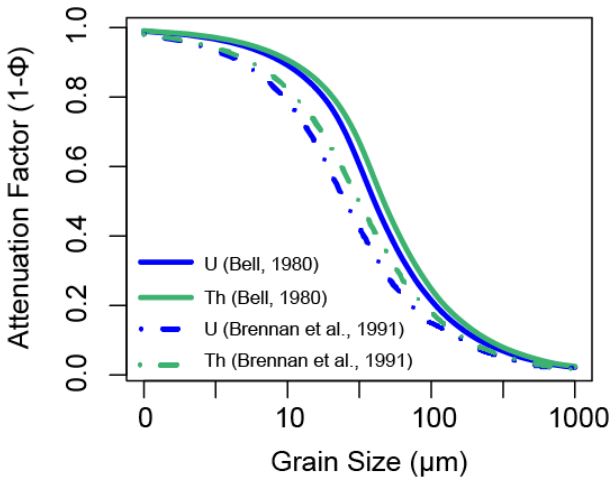

Figure 2: Grain size attenuation factors for $\dot{D}_{\alpha}$, interpolated from the original data of Bell (1980) and Brennan et al. (1991) using a spline fit. The original and fitted data are available in Tables S3.3a and S3.3b.

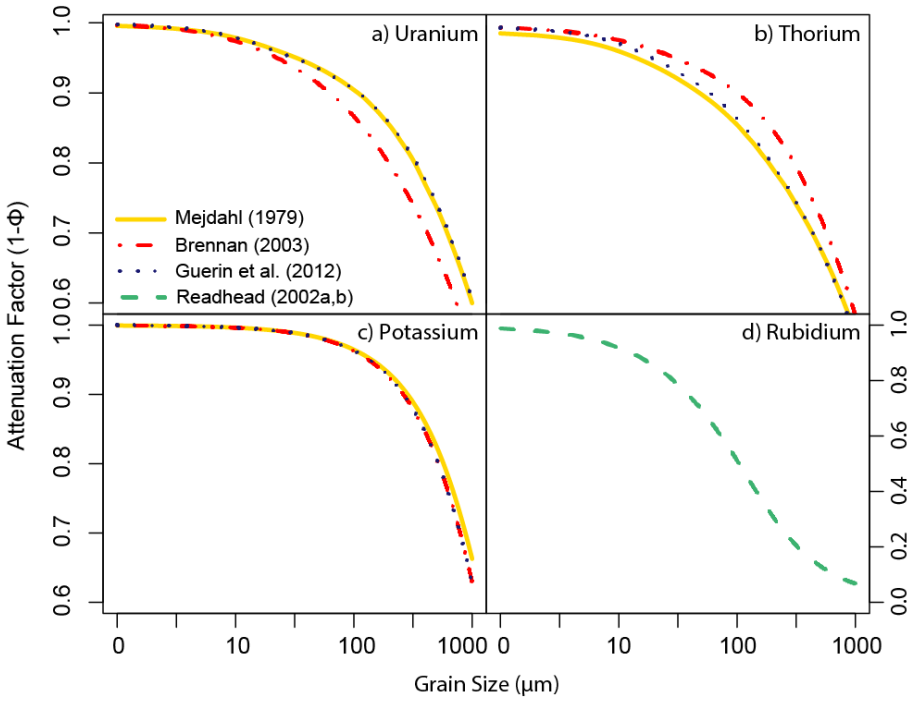

Figure 3: Grain size attenuation factors for $\dot{D}_{\beta}$, interpolated from the original data of Mejdahl, 1979, Brennan, 2003 and Guerin et al., 2012and Readhead, 2002a and Readhead, 2002b. Note that only the quartz factors of Guerin et al. (2012) are shown, but both the quartz and feldspar factors are available for use within DRAC. The original and fitted data are available in Tables S3.4a and S3.4b.

Each of the grain size attenuation datasets has been fitted with a smoothed spline function in RStudio, and datasets have been generated over the grain size range 1–1000 µm. The original and fitted data are provided in the Supplementary Information (Tables S3.3a,b and S3.4a,b). The fitted alpha and beta grain size attenuation factors are summarised in Fig. 2 and Fig. 3 respectively. The attenuation factors ($1 - \Phi(D)$) are used to correct external doses, whilst the absorption factors ($\Phi(D)$) are used for internal doses.

Using the grain size data provided by the user, DRAC calculates the attenuation factor from the minimum and maximum grain size and takes the mean as the grain size attenuation or absorption factor. Quantification of the uncertainties associated with each of the attenuation factor datasets is not discussed

in the various studies, although Brennan (2003) comments that there is a likely uncertainty of several percent for his modelled data, but does not provide a numerical uncertainty estimate. In DRAC, the uncertainty is calculated from half of the absolute difference between the attenuation factors of the minimum and maximum grain sizes.

The decay of radionuclides within the U, Th and K series produce emissions of various energies, and therefore the degree of attenuation by the grain varies according to the relative contributions from these different sources. In DRAC, dose rates are calculated from radionuclide concentrations and conversion factors, or the user can specify a directly measured dose rate. Where radionuclide concentrations (U, Th, K) have been provided, the dose rate arising from each radionuclide is attenuated individually, before being summed to produce the attenuated $\dot{D}_\alpha$ or $\dot{D}_\beta$. If user-defined $\dot{D}_\alpha$ and $\dot{D}_\beta$ values are provided, an average attenuation factor calculated assuming the elemental ratios of Mejdahl (1979) (3 ppm U, 12 ppm Th, 1% K_2O) is used. If no conversion factors have been stipulated because only user defined doses have been provided, DRAC will default to using the most recent conversion factors of Liritzis et al. (2013).

3.3.3. Chemical etching

Chemical etching using hydrofluoric acid is routinely used in the preparation of quartz extracts, both to remove contaminating grains and to remove the majority of the alpha irradiated outer grain margin. It is generally assumed that etching results in removal of an isotropic surface (e.g. Fleming, 1970), however experimental results from Bell and Zimmerman (1978) showed that etching was not uniform for a large proportion of the grains explored (75%) and in some instances resulted in the formation of deep etch pits. Some coarse-grain feldspar preparation protocols also include a chemical etch for the same reason (e.g. Li et al., 2008), although feldspars are known not to etch isotropically (Duller, 1992). Consequently, applying any etch attenuation factor is subject to uncertainty. Bell (1979) and Brennan (2003) have calculated the change in $\dot{D}_\beta$, caused by chemical etching for quartz grains for a range of etch depths. The factors of Bell (1979) are reported as a ratio to the grain size attenuated absorbed dose, and thus can be regarded as secondary etch attenuation factors ($1 - \Phi_{2e}$). In contrast the factors of Brennan (2003) are reported as independent etch attenuation factors ($1 - \Phi_e$) which do not require additional grain size attenuation. To make the different sets of etch attenuation factors comparable, the 100 µm factors of Brennan (2003) are expressed as secondary attenuation factors, achieved through scaling them relative to the 100 µm grain-size attenuation factors also reported in Brennan (2003). At present both of the available secondary etch attenuation factors in DRAC assume an initial grain size of 100 µm, although it should be noted that Brennan (2003) provides factors for a range of grain sizes.

Users of DRAC should provide a sample etch depth range (in µm) and can use the secondary beta etch attenuation factors of either Bell (1979) or Brennan (2003). These datasets have been fitted with a smoothing spline function (Ripley, 2013) over a range of 1–30 µm in RStudio (Tables S3.5a,b and S3.6a,b), and are used to further attenuate the $\dot{D}_\beta$. The uncertainties associated with etch depth attenuation are not discussed by either Bell (1979) or Brennan (2003), and therefore in DRAC, the uncertainty is calculated from half of the absolute difference between the attenuation factors of the minimum and maximum etch depths. Combined secondary etch attenuation factors have also been calculated from the data of Brennan (2003) and Bell (1979) using the elemental ratios of Mejdahl (1979). Note that as Bell (1979) comments that the beta dose from K is negligibly affected by chemical etching, no K etch attenuation is incorporated for the Bell (1979) combined etch attenuation factors. The effect of chemical etching on the beta dose from Rb is not considered although Bell (1979) notes that for an etch of 9 µm depth, the beta dose of Rb is reduced by a factor of 0.755.

Alpha particles penetrate grains of quartz and feldspar to a lesser depth than beta particles. Consequently, the $\dot{D}_\alpha$ is more seriously reduced following chemical etching, and commonly it is assumed that the $\dot{D}_\alpha$ has been completely removed by chemical etching. If users wish to completely ignore any remaining alpha contribution following chemical etching, zero should be input for the a-value. If the a-value is non-zero then the $\dot{D}_\alpha$ remaining following chemical etching will be calculated using the secondary etch attenuation factors of Bell (1979), which are also subject to an assumed grain size of 100 µm. The later factors of Brennan et al. (1991) are not included in DRAC because of limited resolution over the 1–30 µm etch depth range.

3.3.4. Scaling of the gamma dose rate

Conventional sampling strategies for trapped charge dating suggest avoiding sample collection from within 0.3 m of the current sediment surface, which is the range of gamma rays. In near-surface settings the $\dot{D}_\gamma$ should be corrected to take into account the gamma contribution from the sediment matrix, as well as the inert atmosphere above ground level. DRAC offers the option of correcting the $\dot{D}_\gamma$ calculated for samples collected from depths of 0.3 m or less using the scaling factors of Aitken, 1985a and Aitken, 1985b;Table S3.7). For samples within 0.3 m of the surface, the $\dot{D}_\gamma$ from U, Th and K will be individually scaled, unless a user specified $\dot{D}_\gamma$ is provided, in which case the weighted average scaling factor computed by Aitken is applied.

3.3.5. Water content

Water has significant attenuating properties. External $\dot{D}_\alpha$, $\dot{D}_\beta$ and $\dot{D}_\gamma$ must therefore be adjusted for the water content of the sediment from which the sample was taken over the burial lifetime of the sample. The attenuation factors of Aitken and Xin (1990) and Zimmerman (1971) are used in the DRAC calculation, and are 1.49, 1.25 and 1.14 for alpha, beta and gamma radiation respectively. Dose rates are attenuated using the equation of Aitken and Xin (1990) and uncertainties are propagated in quadrature. The water content and uncertainty should be expressed as a percentage and be the weight of water divided by dry sediment: water (%) by mass = (wet mass − dry mass/dry mass) × 100.

3.4. Cosmic dose rate

The contribution from cosmic rays to the total environmental dose rate, whilst small in most depositional settings, is not negligible (Prescott and Hutton, 1994) and should be included as part of the environmental dose rate. The $\dot{D}_c$ calculation is detailed in Prescott and Hutton, 1988 and Prescott and Hutton, 1994 and DRAC uses the calculation protocol outlined in the appendix of Prescott and Hutton (1994; p. 500).Barraboutis and Rustin (1983) observed that the soft component of cosmic rays only penetrates shallow depths of up to 167 $g.cm^{-2}$ (Fig. 4). At greater depths, the $\dot{D}_c$ comprises only the hard (muon) component. In DRAC, the contribution from the soft and hard component will be calculated for samples taken from depths between 0 and 167 $g.cm^{-2}$. At greater depths, only the hard component is calculated (Fig. 4). For $\dot{D}_c$ calculation, DRAC requires the input of the sample depth and the mean overburden density to calculate the $\dot{D}_c$ at a geomagnetic latitude of 55° and 0 m asl. This dose rate is then corrected for the sample-specific geomagnetic latitude and altitude, and users are required to include the latitude, longitude and altitude of the sampling location. Users of DRAC can find a worked example of this calculation in Worksheets S3.9, S3.10, S3.11, along with the look-up table of F, H and J values (Table S3.8) required to correct for location (e.g. Prescott and Stephan, 1982 and Prescott and Hutton, 1994) in the Supplementary Information and on the DRAC website.

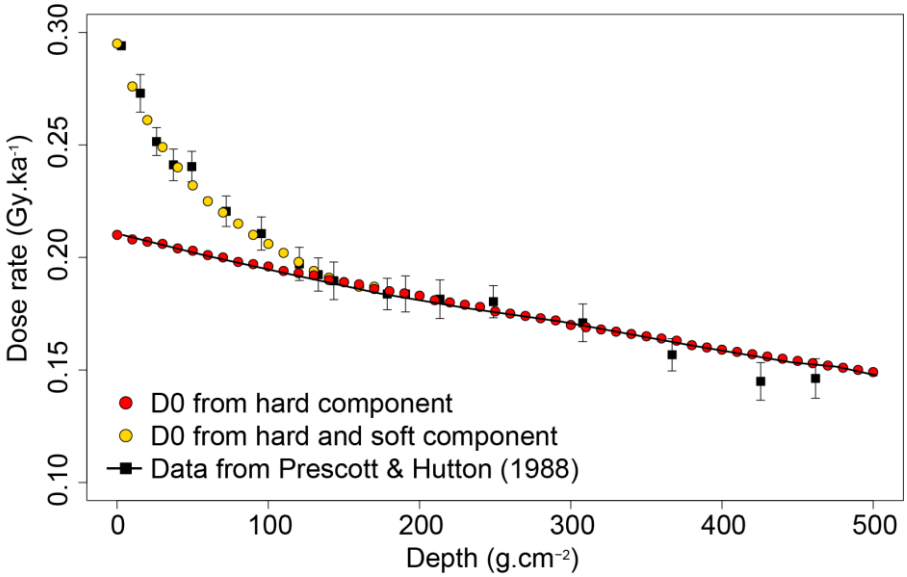

Figure 4: Penetration depths of cosmic rays. The original data from Barbouti and Rastin (1983) as presented in Prescott and Hutton (1988)are shown, together with their fit for the hard component. Data fitted for this study for the contributions from both soft and hard components (depths < 167 g.cm^{-2}) and from hard components only (depths > 167 g.cm^{-2}) are shown.

Cosmic dose rates may fluctuate over longer-term time-scales, due to variability in galactic primary cosmic rays, solar modulation and changes in the geomagnetic dipole moment, although this variability is likely to have averaged out over the past 500 ka (Prescott and Hutton, 1994). To account for possible fluctuations and uncertainties associated with the production of cosmic rays over time, DRAC applies an uncertainty of ±10% to calculated $\dot{D}_c$ values. For more complex depositional settings, users of DRAC also have the option of inputting a user defined $\dot{D}_c$.

3.5. Calculation of Ḋ and age

Ḋ is calculated by combining the attenuated internal and external $\dot{D}_\alpha$ and $\dot{D}_\beta$, the attenuated $\dot{D}_\gamma$ and the $\dot{D}_c$. The values are combined and uncertainties propagated in quadrature. DRAC will also calculate an age if a D_e and uncertainty have been provided, where age = $D_e/\dot{D}$.

4. DRAC comparison

Worked examples of the calculation of DRAC for quartz, feldspar and polymineral samples are provided in the Supplementary Information (Worksheets S3.9, S3.10 and S3.11), along with the DRAC Input and DRAC Output tables (worksheets S3.12 and S3.13). To test Ḋ values calculated by DRAC against published dose rates, Ḋ information was taken from 32 randomly selected studies (totalling 422 samples) and used to calculate Ḋ in DRAC (v1.1). For the 32 studies selected it was necessary to estimate some parameters where they were not detailed in the publication e.g. if the conversion factors used were not stated, the factors of Adamiec and Aitken (1998) were used. Full details of the assumptions made are given in the caption of Fig. 5, which summarises the comparison, presented according to mineral type and grain size. For the full dataset of 422 samples, DRAC and published Ḋ values are in excellent agreement with a ratio of 1.01 ± 0.05. This demonstrates that as a community, Ḋ values are calculated consistently, although some small deviation between DRAC and published Ḋ values is to be expected because of the small variations which will arise from the use of different conversion factors and/or attenuation datasets, some of which have had to be assumed. Sensitivity testing of a quartz sample from Durcan (2012) shows that a ±2% variation

around the calculated value can be generated through the use of different conversion factors, attenuation factors, sample location parameters and uncertainties. Transposition and miscalculation errors have been observed in some publications, which again, leads to discrepancy between the published and DRAC calculated Ḋ values. Despite these various factors, the deviation from unity is slight.

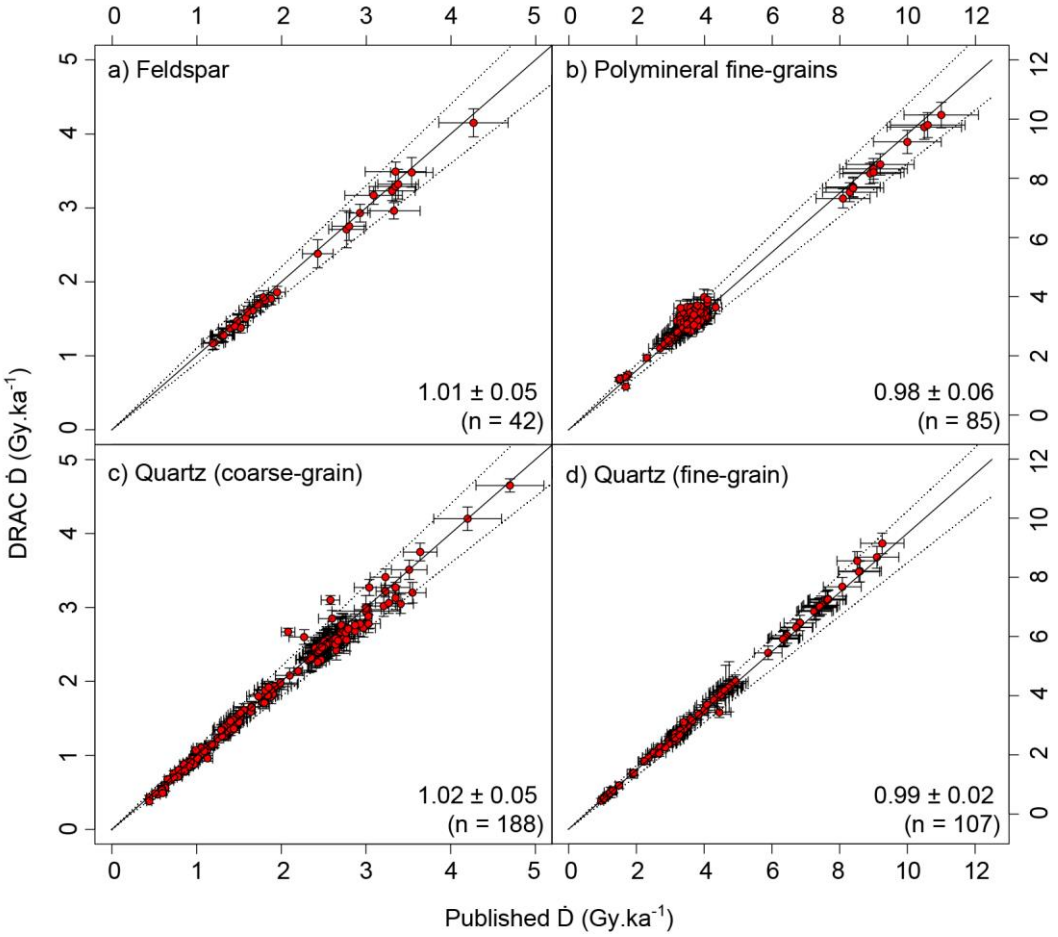

Figure 5: Comparison of dose rates (Ḋ) calculated in DRAC with those previously published. Data are plotted separately for a) feldspar, b) polymineral, c) coarse-grain (>63 µm) quartz and d) fine-grain (<63 µm) quartz. 422 samples from 32 studies are compared with a mean ratio of 1.01 ± 0.05. If not stated in the publication, the following parameters were used to facilitate comparison: conversion factors – Adamiec and Aitken (1998), no Rb calculation from K, grain size attenuation for $\dot{D}_{\alpha}$ and $\dot{D}_{\beta}$ – Bell (1980) and Mejdahl (1979) respectively, etch depth – 9 µm, etch depth attenuation – Bell, 1979, a-value either 0.086 ± 0.0043, 0.035 ± 0.001 (Rees-Jones and Tite, 1997) or 0.15 ± 0.015 (Balescu and Lamothe, 1994) dependent on mineral and grain-size, overburden density – 2.0 ± 0.1 g.cm^{-3}, latitude, longitude and altitude estimated from Google Earth. The studies used for the DRAC comparison: Alappat et al., 2011, Bates et al., 2003, Breman et al., 2003, Buylaert et al., 2007 and Clark-Balzan et al., 2012, Davidovich et al., 2012,Demeter et al., 2012, Fuchs et al., 2012, Haberzettl et al., 2009, Halfen et al., 2010, Hall et al., 2010, Houben et al., 2013, Kaiser et al., 2009, Kars et al., 2012, Kels et al., 2014, Klasen et al., 2011, Kock et al., 2009, Kreutzer et al., 2012, Le Dortz et al., 2009,Lepper et al., 2013, Lomax et al., 2014, Madsen et al., 2009, Roskosch et al., 2012, Schatz et al., 2012, Schmidt et al., 2014,Schokker et al., 2005 and Stevens et al., 2011Tamura et al., 2011, Thiel et al., 2011, Xu et al., 2010 and Yang et al., 2010.

4.1. Reporting Ḋ calculation

The 32 publications used for the DRAC comparison comprises a small proportion of the number of studies investigated for inclusion. This is because the vast majority of publications reviewed did not contain enough basic information to reproduce the Ḋ calculation. We as authors do not wish to dictate a standardised set of data which should be included in journal publications. However, we do ask the community to be mindful of the information necessary to reproduce a Ḋ calculation and to incorporate these details in their publications (or supplementary information) accordingly.

5. Future directions

DRAC is intended to provide a robust and accessible method of dose rate calculation, which enables practitioners to accurately determine environmental dose rates. The website calculations are intended to be transparent and to enable interested parties to recalculate published environmental dose rate values reproducibly. Users may refer to the Supplementary Information and/or DRAC website for an outline of the DRAC calculations and worked examples. It is anticipated that DRAC will facilitate easier inter-laboratory comparisons of environmental dose rate values, through the standardisation of dose rate calculations.

Rather than comprising a final version, it is intended that DRAC will undergo modification as advances in environmental dose rate calculations are made. Potential extensions to the calculator could include the incorporation of Monte-Carlo modelling for beta dose heterogeneity (e.g. Nathan et al., 2003), calculation of gamma dose heterogeneity or the extension of the calculator to other minerals such as calcite. Contributions to DRAC are welcomed and DRAC users are encouraged to contact the authors with updated dose rate datasets, such as conversion and attenuation factors, and/or potential developments to the calculator.

Acknowledgements

Funding from the Quaternary Research Association Outreach Fund has supported the development of this website, and Aberystwyth University is gratefully acknowledged for hosting. JD is supported by the School of Geography and the Environment, University of Oxford. GK acknowledges financial support from the Climate Change Consortium of Wales and Swiss National Fund grant PP00P2-38956. Barry Brennan is thanked for providing his attenuation factor data. Stefan Senk at Senktec (www.senktec.com) designed and built the DRAC website and is thanked for his expertise and creativity. Richard Bailey, Rachel Smedley and participants at the 14th Luminescence and Electron Spin Resonance Dating Conference are thanked for fruitful discussion and suggestions. Corresponding authors JD and GK contributed equally to writing of the manuscript and development of the calculator.

References

Adamiec, G., Aitken, M.J., 1998. Dose-rate conversion factors: update. Ancient TL 16, 37-46.

Aitken, M.J., 1985a. Thermoluminescence Dating. Academic Press, London.

Aitken, M.J., 1985b. Alpha particle effectiveness: numerical relationship between systems. Ancient TL 3, 22-25.

Aitken, M.J., 1998. An Introduction to Optical Dating: The dating of Quaternary sediments by the use of Photon-stimulated Luminescence. Oxford Science Publications, Oxford.

Aitken, M.J., Bowman, S.G.E., 1975. Thermoluminescent dating: assessment of alpha particle contribution. Archaeometry 17, 132-138.

Aitken, M.J., Xie, J., 1990. Moisture correction for annual gamma dose. Ancient TL 8, 6-9.

Alappat, L., Frechen, M., Ramesh, R., Tsukamoto, S., Srinivasalu, S., 2011. Evolution of late Holocene coastal dunes in Cauvery delta region of Tamil Nadu, India. Journal of Asian Earth Sciences, 42, 381-397.

Armitage, S.J., King, G.E., 2013. Optically stimulated luminescence dating of hearths from the Fazzan Basin, Libya: A tool for determining the timing and pattern of Holocene occupation of the Sahara. Quaternary Geochronology 15, 88-97.

Balco, G., Stone, J.O., Lifton, N.A. and Dunai, T.J., 2008. A complete and easily accessible means of calculating surface exposure ages or erosion rates from 10Be and 26Al measurements. Quaternary Geochronology, 3, 174-195.

Balescu, S., Lamothe, M., 1994. Comparison of TL and IRSL age estimates of feldspar coarse grains from waterlain sediments. Quaternary Science Reviews 13, 437-444.

Barbouti, A.I. and Rastin, B.C., 1983. A study of the absolute intensity of muons at sea level and under various thicknesses of absorber. Journal of Physics G: Nuclear Physics, 9, 1577-1595.

Bates, M., Pope, M., Shaw, A., Scott, B., Schwenninger, J.-L., 2003. Late Neanderthal occupation in North-West Europe: rediscovery, investigation and dating of a last glacial sediment sequence at the site of La Cotte de Saint Brelade, Jersey. Journal of Quaternary Science, 28, 647-652.

Bell, W.T., 1979. Attenuation factors for the absorbed radiation dose in quartz inclusions for thermoluminescence dating. Ancient TL 8, 1-12.

Bell, W.T., 1980. Alpha attenuation in Quartz grains for Thermoluminescence Dating. Ancient TL 12, 4-8.

Bell, W.T., Zimmerman, D.W., 1978. The effect of HF acid etching on the morphology of quartz inclusions for thermoluminescence dating. Archaeometry 20, 63-65.

Breman, E., Gillson, L., Willis, K., 2003. How fire and climate shaped grass-dominated vegetation and forest mosaics in northern South Africa during past millennia. The Holocene 22, 1427-1439

Brennan, B.J., 2003. Beta doses to spherical grains. Radiation Measurements 37, 299-303.

Brennan, B.J., Lyons, R.G., Phillips, S.W., 1991. Attenuation of alpha particle track dose for spherical grains. International Journal of Radiation Applications and Instrumentation. Part D. Nuclear Tracks and Radiation Measurements 18, 249-253.

Buylaert, J.-P., Vandenberghe, D., Murray, A.S., Huot, S., De Corte, F., Van den Haute, P., 2007. Luminescence dating of old (>70 ka) Chine loess: A comparison of single-aliquot OSL and IRSL techniques. Quaternary Geochronology, 2, 9-14.

Buylaert, J., Ankjaergaard, C., Murray, A.S., Nielsen, A., 2006. A proposed laboratory intercomparison sample based on a beach-ridge sand from Skagen (Denmark), UK Luminescence and ESR Meeting, Liverpool, UK.

Buylaert, J.P., Murray, A.S., Thomsen, K.J., Jain, M., 2009. Testing the potential of an elevated temperature IRSL signal from K-feldspar. Radiation Measurements 44, 560-565.

Clark-Balzan., Candy, I., Schwenninger, J.-L., Bouzouggar, A., Blockley, S., Nathan, R., Barton, R.N.E., 2012. Coupled U-series and OSL dating of a Late Pleistocene cave sediment sequence, Morocco, North Africa: Significance for constructing Palaeolithic chronologies. Quaternary Geochronology 12, 53-64.

Davidovich, U., Porat, N., Gadot, Y., Avni, Y., Lipschits, O., 2012. Archaeological investigations and OSL dating of terraces at Ramat Rahel, Israel. Journal of Field Archaeology 37, 192-208.

De Corte, F., Vandenberghe, D., Hossain, S.M., De Wispelaere, A., Buylaert, J.-P. and Van den Haute, P., 2007. Preparation and characterization of loess sediment for use as a reference material in the annual radiation dose determination for luminescence dating. Journal of Radioanalytical and Nuclear Chemistry, 272, 2, 311-319.

Demeter, F., Shackelford, L.L., Bacon, A.-M., Duringer, P., Westaway, K., Sayavongkhamdy, T., Braga, J., Sichanthongtip, P., Khamdalavong, P., Ponche, J.-L., Wang, H., Lundstrom, C., Patole-Edoumba, E., Karpoff, A.-M., 2012. Anatomically modern human in Southeast Asia (Laos) by 46 ka. Proceedings of the National Academy of Sciences 109, 14375-14380.

Duller, G.A.T., 1992. Luminescence chronology of raised marine terraces, south-west North Island, New Zealand. Unpublished PhD thesis, University of Wales, Aberystwyth.

Durcan, J.A., 2012. Luminescence dating of sediments in Punjab, Pakistan: implications for the collapse of the Harappan civilisation. Unpublished PhD thesis, Aberystwyth University.

Fleming, S.J., 1970. Thermoluminescent dating: refinement of the quartz inclusion method. Archaeometry, 12, 133-143.

Fuchs, M., Kreutzer, S., Fischer, M., Sauer, D., Sørensen, R., 2012. OSL and IRSL dating of raised beach sand deposits along the southeastern coast of Norway. Quaternary Geochronology 10, 195-200.

Guerin, G., Mercier, N., Adamiec, G., 2011. Dose-rate conversion factors: update. Ancient TL 29, 5-8.

Guerin, G., Mercier, N., Nathan, R., Adamiec, C., Lefrais, Y., 2012. On the use of the infinite matrix assumption and associated concepts: a critical review. Radiation Measurements, 47, 778-785.

Grün, 2009. The “AGE” program for the calculation of luminescence age estimates. Ancient TL 27, 45-46.

Haberzettl, T., Anselmetti, F.S., Bowen, S.W., Fey, M., Mayr, C., Zolitschka, B., Ariztegui, D., Mauz, B., Ohlendorf, C., Kastner, S., Lucke, A., Schabitz, F., Wille, M., 2009. Late Pleistocene dust deposition in the Patagonian steppe – extending and refinding the palaeoenvironmental and tephrochronological record from Laguna Potrok Aike back to 55 ka. Quaternary Science Reviews, 28, 2927-2939.

Halfen, A.F., Gredlund, G.G., Mahan, S.A., 2010. Holocene stratigraphy and chronology of the Casper Dune Field, Casper, Wyoming, USA. The Holocene, 29, 773-783.

Hall, S, A., Miller, M.R., Goble, R.J., 2010. Geochronology of the Bolson sand sheet, New Mexico and Texas, and its archaeological significance. Geological Society of America Bulletin, 122, 1950-1967.

Houben, P., Kühl, N., Dambeck, R., Overath, J., 2013. Lateglacial to Holocene rapid crater infilling of a MIS 2 maar volcano (West-Eifel Volcanic Field, Germany): environmental history and geomorphological feedback mechanisms. Boreas 42, 947-958.

Huntley, D.J., Baril, M.R., 1997. The K content of the K-feldspars being measured in optical dating or in thermoluminescence dating. Ancient TL 15, 11-13.

Jacobs, Z., Wintle, A.G., Duller, G.A.T., 2003. Optical dating of dune sand from Blombos Cave, South Africa: I—multiple grain data. Journal of Human Evolution 44, 599-612.

Kaiser, K., Lai, Z., Schneider, B., Schoch, W.H., She, X., Miehe, G., Bruckner, H., 2009. Sediment sequences and paleosols in the Kyichu Valley, southern Tibet (China), indicating Late Quaternary environmental changes. Island Arc, 18, 404-427.

Kars, R.H., Busschers, F.S., Wallinga, J., 2012. Validating post IR-IRSL dating on K-feldspars through comparison with quartz OSL ages. Quaternary Geochronology 12, 74-86.

Kels, H., Protze, J., Sitlivy, V., Hilgers, A., Zander, A., Anghelinu, M., Bertrams, M., Lehmkuhl, F., In Press. Genesis of loess-like sediments and soils at the foothills of the Banat Mountains, Romania – Examples from the Paleolithic sites Românești and Coşava. Quaternary International, 351, 213-230.

Klasen, N., Engle, M., Bruckner, H., Hausleiter, A., Intilia, A., Eichmann, R., al-Najem, M.H., al-Said, S.F., 2011. Optically stimulated luminescence dating of the city wall system of ancient Tayma (NW Saudi Arabia). Journal of Archaeological Science, 38, 1818-1826.

Kock, S., Huggenberger, P., Preusser, F., Rentzel, P., Wetzel, A., 2009. Formation and evolution of the Lower Terrace of the Rhine River in the area of Basel. Swiss Journal of Geosciences, 102, 307-321.

Kreutzer, S., Fuchs, M., Meszner, S., Faust, D., 2012. OSL chronostratigraphy of a loess-palaeosol sequence in Saxony/Germany using quartz of different grain sizes. Quaternary Geochronology 10, 102-109.

Kulig G, 2005. Erstellung einer Auswertesoftware zur Altersbestimmung mittels Lumineszenzverfahren unter spezieller Berücksichtigung des Einflusses radioaktiver Ungleichgewichte in der 238U-Zerfallsreihe (Creation of a software for luminescence dating with special attention to the influence of radioactive disequilibria in the 238U decay chain). Technische Bergakademie Freiberg, Freiberg unpublished Bsc thesis.

Lai, Z.P., Zöller, L., Fuchs, M., Brückner, H., 2008. Alpha efficiency determination for OSL of quartz extracted from Chinese loess. Radiation Measurements 43, 767-770.

Lang, A., 1994. Infra-red stimulated luminescence dating of Holocene reworked silty sediments. Quaternary Geochronology 13, 525-528.

Le Dortz, K., Meyer, B., Sebrier, M., Nazari, H., Braucher, R., Fattahi, M, Benedetti, L., Foroutan, M., Siame, L., Bourles, D., Talebian, M., Bateman, M.D., Ghoraishi, M., 2009. Holocene right-slip rate determined by cosmogenic and OSL dating on the Anar fault, Central Iran. Geophysics Journal International, 179, 700-710.

Lepper, K., Buell, A.W., Fisher, T.G., Lowell, T.V., 2013. A chronology for glacial Lake Agassiz shorelines along Upham's namesake transect. Quaternary Research 80, 88-98.

Li, B., Li, S.-H., Wintle, A.G., Zhao, H., 2008. Isochron dating of sediments using luminescence of K-feldspar grains. Journal of Geophysical Research: Earth Surface 113, F02026.

Liritzis, I., Stamoulis, K., Papachristodoulou, C., Ioannides, K., 2013. A re-evaluation of radiation dose-rate conversion factors. Mediterranean Archaeology and Archaeometry 13, 1-15.

Lomax, J., Fuchs, M., Freusser, F., Fiebig, M., 2014. Luminescence based loess chronostratigraphy of the Upper Palaeolithic site Krems-Wachtberg, Austria. Quaternary International, 351, 88-97.

Madsen, A.T., Duller, G.A.T., Donnelly, J.P., Roberts, H.M., Wintle, A.G., 2009. A chronology of hurricane landfalls at Little Sippewissett Marsh, Massachusetts, USA, using optical dating. Geomorphology, 109, 36-45.

Mauz, B., Packman, S., Lang, A., 2006. The alpha effectiveness in silt-sized quartz: New data obtained by single and multiple aliquot protocols. Ancient TL 24, 47-52.

Mejdahl, V., 1979. Thermoluminescence Dating: Beta-Dose Attenuation in Quartz Grains. Archaeometry 21, 61-72.

Mejdahl, V., 1987. Internal radioactivity in quartz and feldspar grains. Ancient TL 5, 10-17.

Murray, A.S., Buylaert, J-P, Thiel, Christine, 2015. A Luminescence Dating Intercomparison Based on a Danish Beach-ridge Sand. Radiation Measurements, in press.

Nathan, R.P., Thomas, P.J., Jain, M., Murray, A.S., Rhodes, E.J., 2003. Environmental dose rate heterogeneity of beta radiation and its implications for luminescence dating: Monte Carlo modelling and experimental validation. Radiation Measurements 37, 305-313.

Olley, J., Caitcheon, G., Murray, A., 1998. The distribution of apparent dose as determined by Optically Stimulated Luminescence in small aliquots of fluvial quartz: Implications for dating young sediments. Quaternary Science Reviews 17, 1033-1040.

Prescott, J.R. and Hutton, J.T., 1988. Cosmic ray and gamma ray dosimetry for TL and ESR. Nuclear Tracks and Radiation Measurements, 14, 223-227.

Prescott, J.R. and Hutton, J.T., 1994. Cosmic ray contributions to dose rates for luminescence and ESR dating: Large depths and long-term time variations. Radiation Measurements, 23, 497-500.

Prescott, J.R. and Stephan, L.G., 1982. The contribution of cosmic radiation to the environmental dose for thermoluminescence dating. PACT, 6, 17-25

Readhead, M.L., 2002a. Absorbed dose fraction for 87Rb beta particles. Ancient TL, 20, 25-29.

Readhead, M.L., 2002b. Appendum to “Absorbed dose fraction for 87Rb beta particles”. Ancient TL, 20, 47.

Rees-Jones, J. and Tite, M.S., 1997. Optical dating results for British archaeological sediments. Archaeometry, 39, 177-187.

Rees-Jones, J., 1995. Optical dating of young sediments using fine-grained quartz. Ancient TL 13, 9-14.

Ripley, B., 2013. pspline: Penalized Smoothing Splines. R package version 1.0-16. S original by Jim Ramsey. http://CRAN.R-project.org/package=pspline

Roskosch, J., Tsukamoto, S., Meinsen, J., Frechen, M., Winsemann, J., 2012. Luminescence dating of an Upper Pleistocene alluvial fan and aeolian sandsheet complex: The Senne in the Münsterland Embayment, NW Germany. Quaternary Geochronology 10, 94-101.

Schatz, A.-K., Buylaert, J.-P., Murray, A., Stevens, T., Scholten, T., 2012. Establishing a luminescence chronology for a palaeosol-loess profile at Tokaj (Hungary): A comparison of quartz OSL and polymineral IRSL signals. Quaternary Geochronology 10, 68-74.

Schmidt, E, D., Tsukamoto, S., Frechen, M., Murray, A.S., 2014. Elevated temperature IRSL dating of loess sections in the East Eifel region of Germany. Quaternary International, 334-335, 141-154.

Schokker, J., Cleveringa, P., Murray, A.S., Wallinga, J., Westerhoff, W.E., 2005. An OSL dated Middle and Late Quaternary sedimentary record in the Roer Valley Graben (southeastern Netherlands). Quaternary Science Reviews 24, 2243-2264.

Smedley, R.K., Duller, G.A.T., Pearce, N.J.G., Roberts, H.M., 2012. Determining the K-content of single-grains of feldspar for luminescence dating. Radiation Measurements 47, 790-796.

Spooner, N.A., Aitken, M.J., Smith, B.W., Franks, M., McElroy, C., 1990. Archaeological dating by infrared-stimulated luminescence using a diode array. Radiation Protection Dosimetry 34, 83-86.

Stevens, T., Markovic, S.B., Zech, M., Hambach, U., Sumegi, P., 2011. Dust deposition and climate in the Carpathian Basin over an independently dated last glacial-interglacial cycle. Quaternary Science Reviews, 30, 662-681.

Sutton, S.R., Zimmerman, D.W., 1978. Thermoluminescence dating: radioactivity in quartz. Archaeometry 20, 66-88.

Tamura, T., Bateman, M.D., Kodama, Y., Saitoh, Y., Watanabe, K., Yamaguchi, N., Matsumoto, D., 2011. Building of shore-oblique transverse dune ridges revealed by ground-penetrating radar and optical dating over the last 500 years on Tottori coast, Japan Sea. Geomorphology, 132, 153-166.

Thiel, C., Buylaert, J.-P., Murray, A.S., Terhorst, B., Hofer, B., Tsukamoto, S., Frechen, M., 2011. Luminescence dating of the Stratzing loess profile (Austria) – Testing the potential of an elevated temperature post-IR IRSL protocol. Quaternary International, 234, 23-31.

Thomsen, K.J., Murray, A.S., Jain, M., Bøtter-Jensen, L., 2008. Laboratory fading rates of various luminescence signals from feldspar-rich sediment extracts. Radiation Measurements 43, 1474-1486.

Vandenberghe, D., De Corte, F., Buylaert, J.-P., Kučera, J. and Van Den Haute, P., 2008. On the internal radioactivity in quartz. Radiation Measurements, 43, 771-775.

Xu, L., Ou, X., Lai, Z., Zhou, S., Wang, J., Fu, Y., 2010. Timing and style of Late Pleistocene glaciation in the Queer Shan, northern Hengduan Mountains in the eastern Tibetan Plateau. Journal of Quaternary Science 25, 957-966.

Yang, L., Zhou, J., Lai, Z., Long, H., Zhang, J., 2010. Late glacial and Holocene dune evolution in the Horqin dunefield of northeastern China based on luminescence dating. Palaeogeography, palaeoclimatology, palaeoecology, 296, 44-51.

Zimmerman, D.W., 1971. Thermoluminescent dating using fine grains from pottery. Archaeometry 13, 29-52.

Supplementary Information

Table S1: The inputs required for a DRAC (v1.1) calculation. Users can use this table to guide the input of data into the DRAC input template.

Table Input	Name	Required	Description
TI:1	Project ID	Y	Inputs can be alphabetic, numeric or selected symbols (/ - () [] _). Spaces are not permitted.
TI:2	Sample ID	Y	
TI:3	Mineral	Y	The mineral used for dating: quartz, feldspar or polymineral. Input must be "Q", "F" or "PM".
TI:4	Conversion factors	N	The conversion factors required to calculate dose rates from radionuclide concentrations. Users have the option of datasets from Adamiec and Aitken (1998), Guerin et al. (2011) or Liritzis et al. (2013). Input must be "AdamiecAitken1998", "Guerinetal2011", "Liritzisetal2013" or "X" if conversion factors are not required.
TI:5	External U (ppm)	N	Radionuclide concentrations in parts per million for uranium, thorium and rubidium and % for potassium. Inputs must be 0 or positive and should not be left blank.
TI:6	External δU (ppm)	N	
TI:7	External Th (ppm)	N	
TI:8	External δTh (ppm)	N	
TI:9	External K (%)	N	
TI:10	External δK (%)	N	
TI:11	External Rb (ppm)	N	
TI:12	External δRb (ppm)	N	
TI:13	Calculate external Rb from K conc?	N	Option to calculate a rubidium concentration from potassium, using the 270:1 ratio suggested by Mejdahl (1987). Input should be yes "Y" or no "N".
TI:14	Internal U (ppm)	N	Internal radionuclide concentrations in parts per million for uranium, thorium and rubidium and % for potassium. Inputs must be 0 or positive and should not be left blank.
TI:15	Internal δU (ppm)	N	
TI:16	Internal Th (ppm)	N	
TI:17	Internal δTh (ppm)	N	
TI:18	Internal K (%)	N	
TI:19	Internal δK (%)	N	
TI:20	Internal Rb (ppm)	N	
TI:21	Internal δRb (ppm)	N	
TI:22	Calculate internal Rb from K conc?	N	Option to calculate an internal rubidium concentration from potassium, using the 270:1 ratio suggested by Mejdahl (1987). Input should be yes "Y" or no "N".
TI:23	User external $\dot{D}_\alpha$ ($Gy.ka^{-1}$)	N	Users may input directly measured values for external alpha, beta and gamma dose rates (in $Gy.ka^{-1}$). Any positive inputs in these fields will override dose rates calculated from radionuclide concentrations. Inputs should be 0 or positive and should not be left blank.
TI:24	User external $\delta\dot{D}_\alpha$ ($Gy.ka^{-1}$)	N	
TI:25	User external $\dot{D}_\beta$ ($Gy.ka^{-1}$)	N	
TI:26	User external $\delta\dot{D}_\beta$ ($Gy.ka^{-1}$)	N	
TI:27	User external $\dot{D}_\gamma$ ($Gy.ka^{-1}$)	N	
TI:28	User external $\delta\dot{D}_\gamma$ ($Gy.ka^{-1}$)	N	
TI:29	User internal $\dot{D}$ ($Gy.ka^{-1}$)	N	Users may input an internal dose rate (either alpha, beta or the sum of the two, in $Gy.ka^{-1}$). DRAC will assume that this value

TI:30	User internal δḊ ($Gy.ka^{-1}$)	N	has already been corrected for attenuation. Inputs in this field will override dose rates calculated from radionuclide concentrations. Inputs should be 0 or positive and not left blank.
TI:31	Scale $\dot{D}_\gamma$ at shallow depths?	N	Users may choose to scale gamma dose rates for samples taken within 0.3 m of the ground surface. The scaling factors of Aitken (1985) are used. Input should be yes "Y" or no "N".
TI:32	Grain size min (µm)	Y	The grain size range analysed. DRAC can be used for the grain size ranges between 1 and 1000 µm. Inputs should range between 1 and 1000 and not be left blank.
TI:33	Grain size max (µm)	Y	
TI:34	α-Grain size attenuation factors	Y	The grain size attenuation factors for the alpha dose rate. Users have the option of datasets from Bell (1980) and Brennan et al. (1991). Input must be "Bell1980" or "Brennanetal1991".
TI:35	β-Grain size attenuation factors	Y	The grain size attenuation factors for the beta dose rate. Users have the option of datasets from Mejdahl (1979), Brennan (2003) and Guerin et al. (2012) for quartz or feldspar. Input must be "Mejdahl1979", "Brennan2003", "Guerinetal2012-Q" or "Guerinetal2012-F" .
TI:36	Etch depth min (µm)	Y	The user defined etch depth range (µm). Inputs should range between 0 and 30 and not be left blank.
TI:37	Etch depth max (µm)	Y	
TI:38	β-Etch attenuation factor	N	The etch depth attenuation factors for the beta dose rate. Users have the option of datasets from Bell (1979) and Brennan (2003). Input must be "Bell1979" or "Brennan2003". Note: only the dataset of Bell (1980) is provided for attenuation of the alpha dose rate by etching.
TI:39	a-value	N	Alpha track efficiency value and uncertainty defined by the user. Inputs should be 0 or positive and not left blank.
TI:40	δa-value	N	
TI:41	Water content (%)	Y	Sediment water content (%) over the burial period. Inputs should be 0 or positive and not be left blank.
TI:42	δWater content (%)	Y	
TI:43	Depth (m)	N	Depth and uncertainty from which sample was extracted beneath the ground surface. Inputs should be 0 or positive and not left blank. If user defined Ḋc will be used then an "X" must be input
TI:44	δDepth (m)	N	
TI:45	Overburden density ($g.cm^{-3}$)	N	Density of the overlying sediment matrix from which the sample was taken. Inputs should be 0 or positive and not be left blank. If user defined Ḋc will be used then an "X" must be input
TI:46	δOverburden density ($g.cm^{-3}$)	N	
TI:47	Latitude (decimal degrees)	N	Latitude and longitude of sample location (in degree decimals). Positive values should be used for northern latitudes and eastern longitudes and negative values for south latitudes and western longitudes. Inputs should range from – 90 to 90° for latitudes and -180 to 180° for longitude. If user defined Ḋc will be used then an "X" must be input
TI:48	Longitude (decimal degrees)	N	
TI:49	Altitude (m asl)	N	Altitude of sample location in metres above sea level. Input should be less than 5000 and not left blank. If user defined Ḋc will be used then an "X" must be input
TI:50	User defined $\dot{D}_c$ ($Gy.ka^{-1}$)	N	Users may input a cosmic dose rate (in $Gy.ka^{-1}$). Inputs in these fields will override the DRAC calculated cosmic dose rate. Inputs should be positive or "X" if not required, and not left blank.
TI:51	User defined $\delta\dot{D}_c$ ($Gy.ka^{-1}$)	N	
TI:52	D_e (Gy)	N	Sample D_e and uncertainty (in Gy). Inputs should be positive or "X" if not required, and not left blank.
TI:53	δD_e (Gy)	N	

Table S2: The outputs generated during the DRAC (v1.1) calculation. In the output file created by DRAC, all inputs and outputs are provided.

Table Output	Name	Description
TO:A	External U $\dot{D}_{\alpha}$ (Gy.ka^{-1})	The calculated external dose rates from the provided radionuclide concentrations and selected conversion factors.
TO:B	External δU $\dot{D}_{\alpha}$ (Gy.ka^{-1})	
TO:C	External U $\dot{D}_{\beta}$ (Gy.ka^{-1})	
TO:D	External δU $\dot{D}_{\beta}$ (Gy.ka^{-1})	
TO:E	External U $\dot{D}_{\gamma}$ (Gy.ka^{-1})	
TO:F	External δU $\dot{D}_{\gamma}$ (Gy.ka^{-1})	
TO:G	External Th $\dot{D}_{\alpha}$ (Gy.ka^{-1})	
TO:H	External δTh $\dot{D}_{\alpha}$ (Gy.ka^{-1})	
TO:I	External Th $\dot{D}_{\beta}$ (Gy.ka^{-1})	
TO:J	External δTh $\dot{D}_{\beta}$ (Gy.ka^{-1})	
TO:K	External Th $\dot{D}_{\gamma}$ (Gy.ka^{-1})	
TO:L	External δTh $\dot{D}_{\gamma}$ (Gy.ka^{-1})	
TO:M	External K $\dot{D}_{\beta}$ (Gy.ka^{-1})	
TO:N	External δK $\dot{D}_{\beta}$ (Gy.ka^{-1})	
TO:O	External K $\dot{D}_{\gamma}$ (Gy.ka^{-1})	
TO:P	External δK $\dot{D}_{\gamma}$ (Gy.ka^{-1})	
TO:Q	External Rb $\dot{D}_{\beta}$ (Gy.ka^{-1})	
TO:R	External δRb $\dot{D}_{\beta}$ (Gy.ka^{-1})	
TO:S	Internal U $\dot{D}_{\alpha}$ (Gy.ka^{-1})	The calculated internal dose rates from the provided radionuclide concentrations and selected conversion factors.
TO:T	Internal δU $\dot{D}_{\alpha}$ (Gy.ka^{-1})	
TO:U	Internal U $\dot{D}_{\beta}$ (Gy.ka^{-1})	
TO:V	Internal δU $\dot{D}_{\beta}$ (Gy.ka^{-1})	
TO:W	Internal Th $\dot{D}_{\alpha}$ (Gy.ka^{-1})	
TO:X	Internal δTh $\dot{D}_{\alpha}$ (Gy.ka^{-1})	
TO:Y	Internal Th $\dot{D}_{\beta}$ (Gy.ka^{-1})	
TO:Z	Internal δTh $\dot{D}_{\beta}$ (Gy.ka^{-1})	
TO:AA	Internal K $\dot{D}_{\beta}$ (Gy.ka^{-1})	
TO:AB	Internal δK $\dot{D}_{\beta}$ (Gy.ka^{-1})	
TO:AC	Internal Rb $\dot{D}_{\beta}$ (Gy.ka^{-1})	
TO:AD	Internal δRb $\dot{D}_{\beta}$ (Gy.ka^{-1})	
TO:AE	U $\dot{D}_{\gamma}$ scaling factor	The scaling factors of Aitken (1985) used to correct gamma dose rates of samples taken from within 0.3 m of the ground surface.
TO:AF	Th $\dot{D}_{\gamma}$ scaling factor	
TO:AG	K $\dot{D}_{\gamma}$ scaling factor	
TO:AH	Average $\dot{D}_{\gamma}$ scaling factor	
TO:AI	Depth scaled U $\dot{D}_{\gamma}$ (Gy.ka^{-1})	The gamma dose rates and uncertainties corrected for shallow depth (<0.3 m).
TO:AJ	Depth scaled δU $\dot{D}_{\gamma}$ (Gy.ka^{-1})	
TO:AK	Depth scaled Th $\dot{D}_{\gamma}$ (Gy.ka^{-1})	
TO:AL	Depth scaled δTh $\dot{D}_{\gamma}$ (Gy.ka^{-1})	
TO:AM	Depth scaled K $\dot{D}_{\gamma}$ (Gy.ka^{-1})	
TO:AN	Depth scaled δK $\dot{D}_{\gamma}$ (Gy.ka^{-1})	
TO:AO	Depth scaled user external $\dot{D}_{\gamma}$ (Gy.ka^{-1})	
TO:AP	Depth scaled δuser external $\dot{D}_{\gamma}$ (Gy.ka^{-1})	
TO:AQ	External infinite matrix $\dot{D}_{\alpha}$ (Gy.ka^{-1})	The infinite matrix external and internal dose rates. Calculated either from the radionuclide concentrations and conversion factors or the user defined dose rates. These
TO:AR	External infinite matrix $\delta\dot{D}_{\alpha}$ (Gy.ka^{-1})	
TO:AS	External infinite matrix $\dot{D}_{\beta}$ (Gy.ka^{-1})	

TO:AT	External infinite matrix $\delta\dot{D}_{\beta}$ (Gy.ka^{-1})	values are used as the basis for all subsequent calculations.
TO:AU	External infinite matrix $\dot{D}_{\gamma}$ (Gy.ka^{-1})	
TO:AV	External infinite matrix $\delta\dot{D}_{\gamma}$ (Gy.ka^{-1})	
TO:AW	Internal infinite matrix $\dot{D}_{\alpha}$ (Gy.ka^{-1})	
TO:AX	Internal infinite matrix $\delta\dot{D}_{\alpha}$ (Gy.ka^{-1})	
TO:AY	Internal infinite matrix $\dot{D}_{\beta}$ (Gy.ka^{-1})	
TO:AZ	Internal infinite matrix $\delta\dot{D}_{\beta}$ (Gy.ka^{-1})	
TO:BA	U Alpha grain size attenuation factor	The alpha grain size attenuation factors and uncertainties calculated from the selected dataset and for the specified grain size range. The value is calculated as the average of the attenuation factors for the two grain size extremes and the uncertainty is 50% of the range. If dose rates are calculated using radionuclide concentrations, they are attenuated individually. If a dose rate is provided by the user, it is attenuated using the combined attenuation factor.
TO:BB	δU Alpha grain size attenuation factor	
TO:BC	Th Alpha grain size attenuation factor	
TO:BD	δTh Alpha grain size attenuation factor	
TO:BE	Combined alpha grain size attenuation factor	
TO:BF	δCombined alpha grain size attenuation factor	
TO:BG	U Alpha grain size absorption factor	The alpha grain size absorption factors and uncertainties calculated from the selected dataset and for the specified grain size range. The value is calculated as the average of the attenuation factors for the two grain size extremes and the uncertainty is 50% of the range.
TO:BH	δU Alpha grain size absorption factor	
TO:BI	Th Alpha grain size absorption factor	
TO:BJ	δTh Alpha grain size absorption factor	
TO:BK	Grain size corrected external U $\dot{D}_{\alpha}$ (Gy.ka^{-1})	The external and internal alpha dose rates corrected for grain size attenuation and absorption.
TO:BL	Grain size corrected external δU $\dot{D}_{\alpha}$ (Gy.ka^{-1})	
TO:BM	Grain size corrected external Th $\dot{D}_{\alpha}$ (Gy.ka^{-1})	
TO:BN	Grain size corrected external δTh $\dot{D}_{\alpha}$ (Gy.ka^{-1})	
TO:BO	Grain size corrected user external $\dot{D}_{\alpha}$ (Gy.ka^{-1})	
TO:BP	Grain size corrected user external $\delta\dot{D}_{\alpha}$ (Gy.ka^{-1})	
TO:BQ	Grain size corrected internal U $\dot{D}_{\alpha}$ (Gy.ka^{-1})	
TO:BR	Grain size corrected internal δU $\dot{D}_{\alpha}$ (Gy.ka^{-1})	
TO:BS	Grain size corrected internal Th $\dot{D}_{\alpha}$ (Gy.ka^{-1})	
TO:BT	Grain size corrected internal δTh $\dot{D}_{\alpha}$ (Gy.ka^{-1})	
TO:BU	U Beta grain size attenuation factor	The beta grain size attenuation factors and uncertainties calculated from the selected dataset and for the specified grain size range. The value is calculated as the average of the attenuation factors for the two grain size extremes and the uncertainty is 50% of the range. If dose rates are calculated using radionuclide concentrations, they are attenuated individually. If a dose rate is provided by the user, it is attenuated using the combined attenuation factor based on the ratio of Mejdahl (1979).
TO:BV	U δBeta grain size attenuation factor	
TO:BW	Th Beta grain size attenuation factor	
TO:BX	Th δBeta grain size attenuation factor	
TO:BY	K Beta grain size attenuation factor	
TO:BZ	K δBeta grain size attenuation factor	
TO:CA	Rb Beta grain size attenuation factor	
TO:CB	Rb δBeta grain size attenuation	

	factor	
TO:CC	Compiled beta grain size attenuation factor	
TO:CD	δCompiled beta grain size attenuation factor	
TO:CE	U Beta grain size absorption factor	The beta grain size absorption factors and uncertainties calculated from the selected dataset and for the specified grain size range. The value is calculated as the average of the attenuation factors for the two grain size extremes and the uncertainty is 50% of the range.
TO:CF	U δBeta grain size absorption factor	
TO:CG	Th Beta grain size absorption factor	
TO:CH	Th δBeta grain size absorption factor	
TO:CI	K Beta grain size absorption factor	
TO:CJ	K δBeta grain size absorption factor	
TO:CK	Rb Beta grain size absorption factor	
TO:CL	Rb δBeta grain size absorption factor	
TO:CM	Grain size corrected external U $\dot{D}_\beta$ ($Gy.ka^{-1}$)	The external and internal beta dose rates corrected for grain size attenuation and absorption.
TO:CN	Grain size corrected external δU $\dot{D}_\beta$ ($Gy.ka^{-1}$)	
TO:CO	Grain size corrected external Th $\dot{D}_\beta$ ($Gy.ka^{-1}$)	
TO:CP	Grain size corrected external δTh $\dot{D}_\beta$ ($Gy.ka^{-1}$)	
TO:CQ	Grain size corrected external K $\dot{D}_\beta$ ($Gy.ka^{-1}$)	
TO:CR	Grain size corrected external δK $\dot{D}_\beta$ ($Gy.ka^{-1}$)	
TO:CS	Grain size corrected external Rb $\dot{D}_\beta$ ($Gy.ka^{-1}$)	
TO:CT	Grain size corrected external δRb $\dot{D}_\beta$ ($Gy.ka^{-1}$)	
TO:CU	Grain size corrected user external $\dot{D}_\beta$ ($Gy.ka^{-1}$)	
TO:CV	Grain size corrected user external δ$\dot{D}_\beta$ ($Gy.ka^{-1}$)	
TO:CW	Grain size corrected internal U $\dot{D}_\beta$ ($Gy.ka^{-1}$)	
TO:CX	Grain size corrected internal δU $\dot{D}_\beta$ ($Gy.ka^{-1}$)	
TO:CY	Grain size corrected internal Th $\dot{D}_\beta$ ($Gy.ka^{-1}$)	
TO:CZ	Grain size corrected internal δTh $\dot{D}_\beta$ ($Gy.ka^{-1}$)	
TO:DA	Grain size corrected internal K $\dot{D}_\beta$ ($Gy.ka^{-1}$)	
TO:DB	Grain size corrected internal δK $\dot{D}_\beta$ ($Gy.ka^{-1}$)	
TO:DC	Grain size corrected internal Rb $\dot{D}_\beta$ ($Gy.ka^{-1}$)	
TO:DD	Grain size corrected internal δRb $\dot{D}_\beta$ ($Gy.ka^{-1}$)	
TO:DE	U Alpha etch attenuation factor	The alpha etch depth attenuation factors calculated from the Bell (1980) dataset for the specified etch depth. The value is calculated as the average of the attenuation factors
TO:DF	U δAlpha Etch attenuation factor	
TO:DG	Th Alpha etch attenuation factor	

TO:DH	Th δAlpha etch attenuation factor	for the etch depth extremes and the uncertainty is 50% of the range. If dose rates are calculated using radionuclide concentrations, they are attenuated individually. If a dose rate is provided by the user, it is attenuated using the combined attenuation factor.
TO:DI	Compiled alpha etch attenuation factor	
TO:DJ	δCompiled alpha etch attenuation factor	
TO:DK	U Alpha etch absorption factor	Alpha etch depth absorption factors calculated from the Bell (1980) dataset for the specified etch depth. The value is calculated as the average of the attenuation factors for the etch depth extremes and the uncertainty is 50% of the range.
TO:DL	U δAlpha Etch absorption factor	
TO:DM	Th Alpha etch absorption factor	
TO:DN	Th δAlpha etch absorption factor	
TO:DO	Etch corrected external U $\dot{D}_\alpha$ ($Gy.ka^{-1}$)	The external and internal alpha dose rates corrected for etch depth attenuation and absorption.
TO:DP	Etch corrected external δU $\dot{D}_\alpha$ ($Gy.ka^{-1}$)	
TO:DQ	Etch corrected external Th $\dot{D}_\alpha$ ($Gy.ka^{-1}$)	
TO:DR	Etch corrected external δTh $\dot{D}_\alpha$ ($Gy.ka^{-1}$)	
TO:DS	Etch corrected user external $\dot{D}_\alpha$ ($Gy.ka^{-1}$)	
TO:DT	Etch corrected user external δ$\dot{D}_\alpha$ ($Gy.ka^{-1}$)	
TO:DU	Etch corrected internal U $\dot{D}_\alpha$ ($Gy.ka^{-1}$)	
TO:DV	Etch corrected internal δU $\dot{D}_\alpha$ ($Gy.ka^{-1}$)	
TO:DW	Etch corrected internal Th $\dot{D}_\alpha$ ($Gy.ka^{-1}$)	
TO:DX	Etch corrected internal δTh $\dot{D}_\alpha$ ($Gy.ka^{-1}$)	
TO:DY	U Beta etch attenuation factor	The beta etch depth attenuation factors calculated from the selected dataset. The value is calculated as the average of the attenuation factors for the etch depth extremes and the uncertainty is 50% of the range. The uncertainty is ±2%. If dose rates are calculated using radionuclide concentrations, they are attenuated individually. If a dose rate is provided by the user, it is attenuated using the combined attenuation factor.
TO:DZ	U δBeta etch attenuation factor	
TO:EA	Th Beta etch attenuation factor	
TO:EB	Th δBeta etch attenuation factor	
TO:EC	K Beta etch attenuation factor	
TO:ED	K δBeta etch attenuation factor	
TO:EE	Compiled beta etch attenuation factor	
TO:EF	δCompiled beta etch attenuation factor	
TO:EG	U Beta etch absorption factor	The beta etch depth absorption factors calculated from the selected dataset. The value is calculated as the average of the attenuation factors for the etch depth extremes and the uncertainty is 50% of the range.
TO:EH	U δBeta etch absorption factor	
TO:EI	Th Beta etch absorption factor	
TO:EJ	Th δBeta etch absorption factor	
TO:EK	K Beta etch absorption factor	
TO:EL	K δBeta etch absorption factor	
TO:EM	Etch corrected external U $\dot{D}_\beta$ ($Gy.ka^{-1}$)	The external and internal beta dose rates corrected for etch depth attenuation and absorption.
TO:EN	Etch corrected external δU $\dot{D}_\beta$ ($Gy.ka^{-1}$)	
TO:EO	Etch corrected external Th $\dot{D}_\beta$ ($Gy.ka^{-1}$)	
TO:EP	Etch corrected external δTh $\dot{D}_\beta$ ($Gy.ka^{-1}$)	

TO:EQ	Etch corrected external K $\dot{D}_\beta$ ($Gy.ka^{-1}$)	
TO:ER	Etch corrected external δK $\dot{D}_\beta$ ($Gy.ka^{-1}$)	
TO:ES	Etch corrected user external $\dot{D}_\beta$ ($Gy.ka^{-1}$)	
TO:ET	Etch corrected user external $\delta\dot{D}_\beta$ ($Gy.ka^{-1}$)	
TO:EU	Etch corrected internal U $\dot{D}_\beta$ ($Gy.ka^{-1}$)	
TO:EV	Etch corrected internal δU Dβ ($Gy.ka^{-1}$)	
TO:EW	Etch corrected internal Th $\dot{D}_\beta$ ($Gy.ka^{-1}$)	
TO:EX	Etch corrected internal δTh $\dot{D}_\beta$ ($Gy.ka^{-1}$)	
TO:EY	Etch corrected internal K $\dot{D}_\beta$ ($Gy.ka^{-1}$)	
TO:EZ	Etch corrected internal δK $\dot{D}_\beta$ ($Gy.ka^{-1}$)	
TO:FA	a-value corrected external U $\dot{D}_\alpha$ ($Gy.ka^{-1}$)	The external and internal alpha dose rates corrected for alpha track efficiency using the provided a-value.
TO:FB	a-value corrected external δU $\dot{D}_\alpha$ ($Gy.ka^{-1}$)	
TO:FC	a-value corrected external Th $\dot{D}_\alpha$ ($Gy.ka^{-1}$)	
TO:FD	a-value corrected external δTh $\dot{D}_\alpha$ ($Gy.ka^{-1}$)	
TO:FE	a-value corrected user external $\dot{D}_\alpha$ ($Gy.ka^{-1}$)	
TO:FF	a-value corrected user external $\delta\dot{D}_\alpha$ ($Gy.ka^{-1}$)	
TO:FG	a-value corrected internal U $\dot{D}_\alpha$ ($Gy.ka^{-1}$)	
TO:FH	a-value corrected internal δU $\dot{D}_\alpha$ ($Gy.ka^{-1}$)	
TO:FI	a-value corrected internal Th $\dot{D}_\alpha$ ($Gy.ka^{-1}$)	
TO:FJ	a-value corrected internal δTh $\dot{D}_\alpha$ ($Gy.ka^{-1}$)	
TO:FK	External Dry $\dot{D}_\alpha$ ($Gy.ka^{-1}$)	The external dose rates corrected for grain size and etch depth attenuation.
TO:FL	External Dry $\delta\dot{D}_\alpha$ ($Gy.ka^{-1}$)	
TO:FM	External Dry $\dot{D}_\beta$ ($Gy.ka^{-1}$)	
TO:FN	External Dry $\delta\dot{D}_\beta$ ($Gy.ka^{-1}$)	
TO:FO	External Dry $\dot{D}_\gamma$ ($Gy.ka^{-1}$)	
TO:FP	External Dry $\delta\dot{D}_\gamma$ ($Gy.ka^{-1}$)	
TO:FQ	Water corrected $\dot{D}_\alpha$	The water attenuated external alpha, beta and gamma dose rates.
TO:FR	Water corrected $\delta\dot{D}_\alpha$	
TO:FS	Water corrected $\dot{D}_\beta$	
TO:FT	Water corrected $\delta\dot{D}_\beta$	
TO:FU	Water corrected $\dot{D}_\gamma$ ($Gy.ka^{-1}$)	
TO:FV	Water corrected $\delta\dot{D}_\gamma$ ($Gy.ka^{-1}$)	
TO:FW	Internal Dry $\dot{D}_\alpha$ ($Gy.ka^{-1}$)	The attenuated internal alpha and beta dose rates.
TO:FX	Internal Dry $\delta\dot{D}_\alpha$ ($Gy.ka^{-1}$)	
TO:FY	Internal Dry $\dot{D}_\beta$ ($Gy.ka^{-1}$)	

TO:FZ	Internal Dry $\delta\dot{D}_\beta$ (Gy.ka^{-1})	
TO:GA	$\dot{D}_0$ (Gy.ka^{-1})	The cosmic dose rate calculated at the sample depth, 55°N and sea level.
TO:GB	$\delta\dot{D}_0$ (Gy.ka^{-1})	
TO:GC	Geomagnetic latitude	The geomagnetic latitude calculated from the sample latitude and longitude and sampling depth.
TO:GD	F	The factors required to correct the cosmic dose rate for altitude and geomagnetic latitude (after Prescott and Stefan, 1982).
TO:GE	H	
TO:GF	J	
TO:GG	$\dot{D}_c$ (Gy.ka^{-1})	The calculated or user defined cosmic dose rate used in final environmental dose rate calculation.
TO:GH	$\delta\dot{D}_c$ (Gy.ka^{-1})	
TO:GI	External $\dot{D}$ (Gy.ka^{-1})	DRAC calculated external and internal dose rates.
TO:GJ	External $\delta\dot{D}$ (Gy.ka^{-1})	
TO:GK	Internal $\dot{D}$ (Gy.ka^{-1})	
TO:GL	Internal $\delta\dot{D}$ (Gy.ka^{-1})	
TO:GM	Environmental Dose Rate (Gy.ka^{-1})	DRAC calculated environmental dose rate.
TO:GN	δEnvironmental Dose Rate (Gy.ka^{-1})	
TO:GO	Age (ka)	Age, if D_e is provided, calculated using the DRAC determined dose rate.
TO:GP	δAge (ka)	

Supplementary information 3 is available as a spreadsheet which can be downloaded from the user guide section of the DRAC website.